Fickian and non-Fickian diffusion with bimolecular reactions

Yotam Berkowitz, Yaniv Edery, Harvey Scher, and Brian Berkowitz
Department of Environmental Sciences and Energy Research, Weizmann Institute of Science, Rehovot 76100, Israel
(Received 4 November 2012; published 25 March 2013)

Mixing zone dynamics of a reaction product C during diffusion of two species (A and B) are examined, using a two-dimensional particle tracking model (PT) for the reaction $A + B \rightarrow C$, allowing for both Fickian and non-Fickian transitions. The form of PT we use is equivalent to a continuous time random walk, which is a widely used model for anomalous transport and diffusion. It is shown that the basic patterns of the C dynamics—the temporal evolution of the spatial profile and the temporal C production—are similar for both modes of diffusion. However, the distinctive time scale for the non-Fickian case is very much larger even when the median transition steps are matched with the Fickian case. For immobile C, the spatial profile pattern is a broadening (Gaussian) reaction front evolving to a concentration-fluctuation dominated (Lorentzian) shape. The temporal C production is fit well by a stretched exponential for both diffusion types. In analyzing experiments, the appearance of a Gaussian C profile does not prove that the diffusion process is Fickian.

DOI: 10.1103/PhysRevE.87.032812 PACS number(s): 82.40.Ck, 05.40.Fb, 05.40.Jc, 82.20.Wt

I. INTRODUCTION

Reaction-diffusion problems are a rich source of nonlinear dynamics, manifest in a wide range of systems intensely studied for many years in physics, chemistry, biology, and earth sciences [1–4]. A particular broad interest involves the bimolecular chemical reaction $A + B \rightarrow C$, where A and B denote two reactive species [5–7]. A plethora of modeling studies of bimolecular reactions has appeared over the last three decades [8–12], based mostly on solving partial differential equations (PDEs) and particle tracking (PT) methods. A key feature of recent work has been the inclusion of transport and diffusion in disordered systems into the reaction dynamics. Important examples are studies of the potential of geological formations (porous media) as long-term repositories for nuclear wastes and the sequestration of CO_2.

The combination of species migration (with or without a bias) in a complex (heterogeneous) medium and the encounter modes of chemical reaction has been difficult to model, especially with PDEs [13]. The basic difficulty is the treatment of the effect of fluctuations at multiple scales, which give rise to anomalous (non-Fickian) diffusion [14,15] and the mixing zone evolution of the reacting species. In the PDE approach, it is the very equations one must solve that contain an empirical nonlinear form for the reaction term. For the Fickian case, this term is usually assumed to be a product of the species concentrations $\Gamma c_A(\mathbf{x},t)c_B(\mathbf{x},t)$, where Γ is a reaction constant [16]. For the non-Fickian case, the reaction term for the (nonlocal-in-time) PDE has not been established.

Our theoretical approach to this problem is PT with specific space-time distributions that make the process equivalent to a continuous time random walk (CTRW). We have demonstrated that, in the pure transport (nonreacting) case, using this PT is equivalent to solving the (Fickian) advection-diffusion equation and the (non-Fickian) PDE version of CTRW, depending on the distributions determining the particle advance [17]. The advantage of PT is the natural way one can study the influences of small-scale fluctuations in the species concentrations on reaction mixing and pattern formation [13,18–21]. PT can flexibly model different reaction schemes, e.g., a reaction rule based strictly on the spatial proximities of A and B (without the attendant volume averaging).

II. METHOD OF ANALYSIS

We concentrate on the dynamics of the reaction product C, recording both the temporal C production and the spatial profile over time. In our two-dimensional (2D) computations we consider a square domain with symmetric initial conditions and pulse injection of A and B at two different points along the horizontal center line of the domain. The domain is sufficiently large that the boundaries do not affect the diffusion-reaction patterns. The two species move either by Fickian or non-Fickian diffusion and undergo the bimolecular reaction $A + B \rightarrow C$, where C either precipitates (and is therefore immobile) or remains in solution and diffuses. The reaction is considered instantaneous and irreversible when the species are within a circle of radius R. This step can be generalized easily in a number of ways.

The general method of our PT is described in detail in [19]. Briefly, in this CTRW PT, the movement of each reactant (and product) particle is governed by the equation of motion:

$$\mathbf{s}^{(N+1)} = \mathbf{s}^{(N)} + \boldsymbol{\varsigma}^{(N)}, \quad t^{(N+1)} = t^{(N)} + \tau^{(N)}, \tag{1}$$

where a random spatial increment $\boldsymbol{\varsigma}^{(N)}$ and a random temporal increment $\tau^{(N)}$ are assigned to each particle transition, according to the joint transition displacement and time probability density $\psi(\mathbf{s},t)$. The decoupled form $\psi(\mathbf{s},t) = p(\mathbf{s})\psi(t)$ [19], where $\boldsymbol{\varsigma}^{(N)}$ and $\tau^{(N)}$ are chosen from distinct and independent probability density functions (PDFs), has been shown to work well except in the case that $p(\mathbf{s})$ describes a Lévy flight, which we do not consider here. Here, the spatial PDF $p(\mathbf{s})$ is chosen as a normal distribution for s with a radially uniform angular component. The temporal PDF, $\psi(t)$, controls the character of the diffusion: pure Fickian diffusion is obtained by an exponential distribution $\psi(t) = \lambda_t e^{-\lambda_t t}$, with mean $1/\lambda_t$. For non-Fickian diffusion, a truncated power law (TPL) PDF [17] embodies two key characteristics, a power law behavior and a

transition to Fickian:

$$\psi(t) = \frac{n}{t_1} \exp(-t/t_2)/(1 + t/t_1)^{1+\beta}, \quad (2)$$

where

$$n \equiv (t_1/t_2)^{-\beta} \exp(-t_1/t_2)/\,\Gamma(-\beta, t_1/t_2) \quad (3)$$

is a normalization factor; β is a measure of the spectrum; t_1 is a scaling time, e.g., for median transitions between sites; t_2 is a "cutoff" time; and $\Gamma(a,x)$ is the incomplete Gamma function [22]. For transition times $t_1 \ll t \ll t_2$, $\psi(t)$ behaves as a power law $\propto (t/t_1)^{-1-\beta}$, while, for $t \gg t_2$, $\psi(t)$ decreases exponentially; thus a finite t_2 enables smooth evolution from non-Fickian to Fickian transport. Note that anomalous diffusion occurs only for $0 < \beta < 1$, the root mean square (rms) of the plume $\sigma(t) \propto t^{\beta/2}$ [23]; it is normal for $\beta \geqslant 1$. This is a general characterization of anomalous diffusion.

At each sampling time, Δt, all particles in the system are frozen in midflight [19]. If A and B particles are within a reaction radius R, C forms at the midpoint between the particles, and A and B are removed from the system. All possible reactions between A and B particles for that sampling time are allowed to occur. Note that no crowding effects occur as particles diffuse in a 2D continuum. It is evident that R plays a key role in determining the reaction behavior. As R increases, averaging of A and B concentrations increases, and consequently C production increases, concentration fluctuations are suppressed, and the tails of the C profile diminish (in contrast to recent experimental observations, e.g., [19,21,24]). In most cases, the reaction radius was set at $R = 0.1$ μm. The sampling time, Δt, also affects the degree of mixing and reaction and thus that of the formation of C particles. A more continuous accounting of the reactions is achieved for Δt that are sufficiently small.

We choose a diffusion coefficient $D \sim 10^{-9}$ m^2/s, which is representative of an ion such as Na^+ (1.33×10^{-9} m^2/s) or Cl^- (2.03×10^{-9} m^2/s) diffusing in water at 25 °C [25]. For Fickian diffusion, we sample from a normal PDF for the spatial transitions, with mean $\epsilon = 10$ μm and standard deviation $\sigma = 1$ μm. For the temporal transitions, we sample from an exponential distribution with mean transition time $1/\lambda_t$. In a 2D system, $D = \epsilon^2/(4\delta t)$, where ϵ and δt are the mean step length and time, respectively. For $D \sim 10^{-9}$ m^2/s and $\epsilon = 10$ μm, it follows that $\delta t = 1/40$ s. The injection points for A and B particles are separated by 100 μm. The sampling time (i.e., at which the reactions between A and B are determined) is, in most cases, $\Delta t = \frac{1}{5}\delta t = 1/200$ s with a total run time $T = 55$ s. For the non-Fickian diffusion case we choose a value of $\beta = 0.7$ [14], with a large cutoff time $t_2 = 10^4$ s. The influence of t_1 is defined by its role as a scaling factor in the TPL, i.e., $t_1\psi(t) = f(\tau)$, with $\tau = t/t_1$. We set t_1 typically equal to $\delta t = 1/40$ s to have the two types of diffusion at similar time steps. The very large difference in migration time scales between them is then due to the anomalous spreading of the non-Fickian profiles; i.e., the PT results confirm that rms $\sigma \propto t^{\beta/2}$. An important final parameter is the number of particles for each of A and B. Previous analyses [19] confirmed that 50 000 particles yielded representative results (e.g., 100 000 particles yielded identical results). In most cases, we consider particle concentrations normalized by the total number of (A or B) particles.

III. RESULTS

Figure 1 shows the picture of the interactions of the spreading plumes and the difference between the two diffusion cases. In Fig. 1(a), representative plumes of A and B for Fickian diffusion are interpenetrating and interacting, creating islands of C particles, which are initially most dense along the center line. Interestingly, one can observe the survival of individual A particles in the "sea" of B particles (and vice versa). This is in fact one of the key elements of our analysis: PT captures the statistically small fluctuations in concentration that play a significant role in the overall temporal evolution of particle and product concentrations and spatial patterns. Such behavior has been found experimentally (e.g., [24]) and quantified with PT [19,21].

One can glean key features of the reaction from this plot augmented with the C production data of Fig. 2. Basically there is a rapid C production in the initial maximum overlap of A and B, which we designate the reaction front in the representative region 200 ± 25 μm. Analysis of the data shows that the C production in this region peaks at $T = 1$ s and subsequently decays due to exhausting A and B in the region. Meanwhile the C production outside this region grows and peaks at $T = 3$ s due to the dispersing of A in the B peak area and vice versa.

We examine this reaction dynamic in further detail. We spatially integrate the C islands along the y axis and show it in a comparison with similar plots of the A and B plumes in Fig. 1(b). The same plot is shown in Fig. 1(c) for non-Fickian diffusion at the same time of $T = 2$ s. In Fig. 1(b) one can observe that the peaks of A and B have shifted and the profile is not symmetric about the peak position, with a sharper decline within the reaction front. The tail of the A plume is dispersing in the B plume (and vice versa) outside the reaction front and creating spreading C islands [see Fig. 1(a)] with larger concentration fluctuations. This overlap is due to random encounter in the PT approach. In Fig. 1(c) the plume peaks have not shifted (the peaks are very sharp, characteristic of anomalous or non-Fickian behavior) and the C production is confined strictly to the reaction front. A relative measure of the C production and the diminution of A and B can be seen in Fig. 1(d). We plot the time dependence of the ratios of the peaks (maxima) of the spatially integrated C and A profiles for the two diffusion cases (note the different time scaling of the two curves). We can observe the time evolution of the picture outlined above: for the Fickian case a rapid growth of C with decreasing A and B followed by a surprisingly sharp transition to a decrease in C production with a slower decrease in A and B. The non-Fickian case has the same pattern but on a different time scale—a shift in the peak position by a factor of ~20. Although the median temporal steps between the two cases have been chosen to be the same, the anomalous dynamic manifests the much larger time scale of reaction. It is caused by the admittance in the non-Fickian case of less frequent long transitions compared to the median one. This is characteristic of disorder. The non-Fickian aspect has measurable consequences for recent observations of diffusion in cells (with a $\beta = 0.7$ [14]).

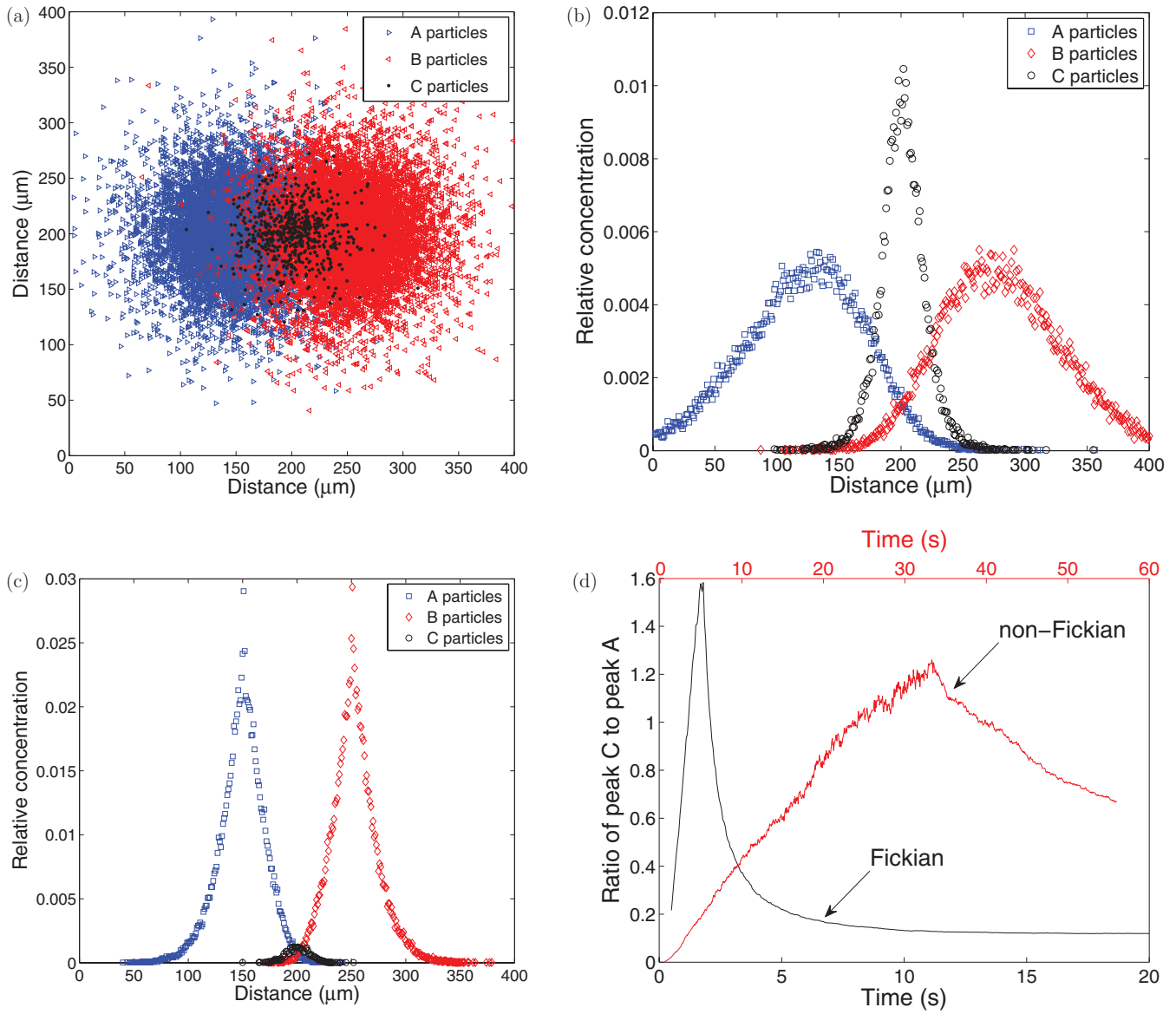

FIG. 1. (Color online) (a) Representative spatial A and B plume patterns, interacting to produce C ($T = 15$ s, with 10 000 particles each of A and B) for Fickian diffusion. (b), (c) Spatially integrated (over the y axis) concentration profiles of A, B, and C particles, at $T = 2$ s, $R = 0.1$ μm, for (b) Fickian diffusion and (c) non-Fickian diffusion with $\beta = 0.7$, $t_1 = 0.025$ s, and $t_2 = 10^4$ s. (d) Ratios of peaks of spatially integrated C profile to A profiles, over time, for Fickian diffusion (lower x axis) and non-Fickian diffusion (upper x axis) with $\beta = 0.7$, $t_1 = 0.025$ s, and $t_2 = 10^4$ s.

The profiles evolution is further evinced in the next two figures. Figure 2 shows the C particle production over time, for the two cases. They are both fit very well with a stretched exponential (SE) function $f(t) = \exp(-at^{\gamma})$ from the peak of each profile with γ =0.2 (Fickian) and γ =0.08 (non-Fickian). Again we observe a sharp transition, with the production decaying faster for the Fickian and becoming comparable to the non-Fickian after $T = 10$ s. At longer times, the curves reach "quasiasymptotic" (transient, not steady-state) values and subsequently converge to zero as there are a fixed number of reactant particles. The convergence is slow, and the remaining (unreacted) A and B particles are approximately uniformly distributed in the region between the two points of injection. At time $T = 20$ s, the numbers of C particles produced (from a maximum of 50 000) are already ∼38 000 and ∼15 000 for the Fickian and non-Fickian diffusion cases, respectively. The SE has a widespread association with "relaxation" phenomena. An important derivation of the SE in this context is in [26], where a model of the first passage time for one "defect" out of N, undergoing anomalous diffusion, to hit the origin is solved [see Fig. 1(a): individual A particles in the denser B particle region and vice versa]. The exponent of the SE in that model is proportional to $S(t)$, the number of distinct sites visited in time t with a equal to defect concentration and $\gamma = \beta$ (in three dimensions). In the present reactive case, the "defects" are B and the target for "relaxation" is A. The $S(t)$ is modified in the reactive field, as the B "defects" may encounter other A particles as they diffuse toward the "target" A; we thus

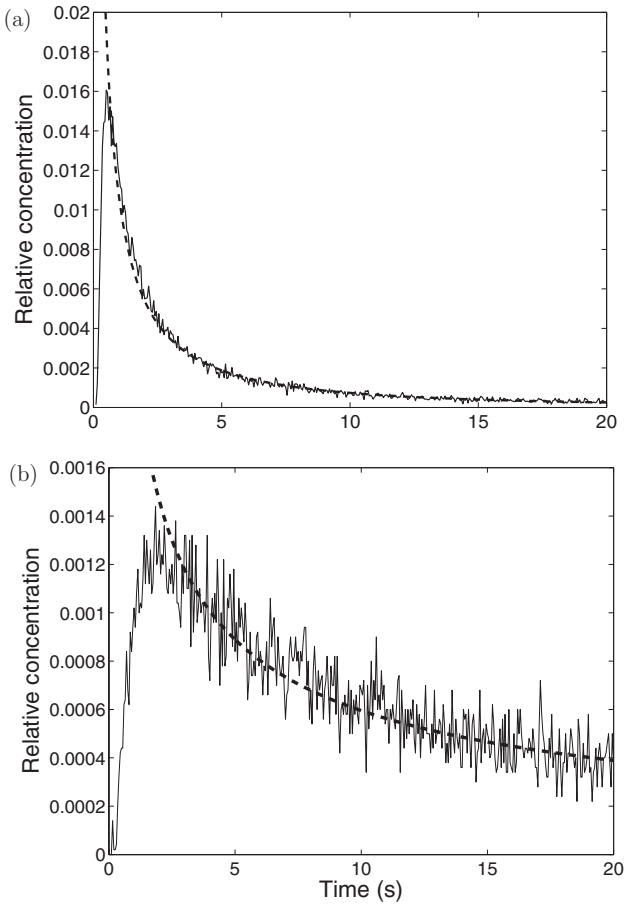

FIG. 2. Production of C particles over time, for (a) Fickian diffusion and (b) non-Fickian diffusion with $\beta = 0.7$, $t_1 = 0.025$ s, and $t_2 = 10^4$ s. Dashed lines show fits of a stretched exponential function (from the peak of each profile), $f(t) = \exp(-at^{\gamma})$, with $a = 4.54$, $\gamma = 0.20$ and $a = 6.17$, $\gamma = 0.08$, respectively, for the Fickian and non-Fickian cases. Note that the y-axis scale for the Fickian case is larger than that for the non-Fickian case.

consider an effective $\gamma < \beta$. Hence we expect $\gamma < 1$ even for the Fickian diffusion.

The decreases in relative concentrations of A particles (identical behavior holds for the B particles, due to the symmetry of the system), for Fickian and non-Fickian diffusion, are shown in Fig. 3. As for the C concentrations (after the peak) shown in Fig. 2, the decreases in A and B concentrations over time are considerably slower for the case of non-Fickian diffusion.

Figure 4 shows the C particle profiles (for immobile C) at times $T = 2$ and 15 s, for Fickian diffusion [Figs. 4(a) and 4(b)] and non-Fickian diffusion, with $\beta = 0.7$ [Figs. 4(c) and 4(d)]. The expectation in light of the discussions of Figs. 1 and 2 is for the C profiles to follow a two-time regime evolution. At short times ($T \leqslant 2$ s) in Fig. 4(a), the profile should reflect rapid compact growth in the reaction front region. The good fit to a Gaussian as shown confirms this behavior. As the C decreases due to sharpening decrease of A and B, the C production builds up outside the reaction front region [see Fig. 1(a)] and the spatial extent of the profile spreads, as is evident in tails heavier than the Gaussian in Fig. 4(b). As the production spatially

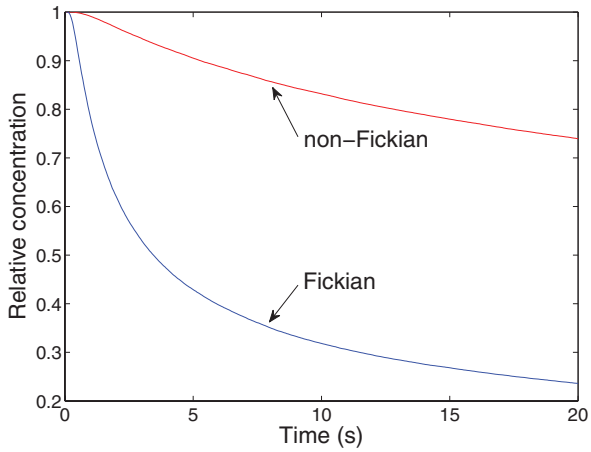

FIG. 3. (Color online) Decrease in relative concentration of A (or B) particles over time, for Fickian diffusion and non-Fickian diffusion with $\beta = 0.7$, $t_1 = 0.025$ s, and $t_2 = 10^4$ s, corresponding to the temporal C production shown in Fig. 2.

spreads, so do the concentration fluctuations. Indicative of this, we quantitatively capture it with a Lorentzian curve. Over the same time range, the non-Fickian C profile remains a Gaussian functional form [Figs. 4(c) and 4(d)].

Hence, the C profile for Fickian diffusion is an evolving one, transiting from a compact Gaussian to a heavy tailed Lorentzian. In order to gain a measure of this transiting we closely estimate this stable distribution by the weighted sum of the stable distributions of a Gaussian and a Lorentzian:

$$a \exp[-|x - 200|^2/(4dt^{\alpha})] + b/[1 + c|x - 200|^2/(dt^{\alpha})], \quad (4)$$

where a, b, c, d, and α are fitting constants. The relative weighting a/b is the key parameter of interest. Note that when applying this PDF to a profile of pure Fickian diffusing particles, d is the diffusion coefficient D and $\alpha = 1$. However, we apply the PDF here to the profiles of generated C particles, so that these constants may take on different values. In our analysis, we find good fits to the C profiles, choosing $\alpha = 1$ for Fickian diffusion and $\alpha = 0.7$ for non-Fickian diffusion. The numerical values of a/b (see Fig. 4 caption) demonstrate the evolving Lorentzian form for the Fickian case (a and b are approximately equal at $T = 5$ s) and the dominant Gaussian form for the non-Fickian case; however, a/b for the latter is decreasing in time, indicating the same pattern, although on a much larger time scale.

To reiterate, one can conclude from all the figures that the reaction patterns of the two different diffusing species are similar but occurring on very different time scales. This is a distinguishing feature of very anomalous behavior. The Gaussian form is a reaction front behavior [16], basically a broadened delta function. As the reaction proceeds, fluctuations in reactant concentrations increase and contribute to the growth of the Lorentzian shape. The very long time scale of the non-Fickian reactions precludes a clear emergence of fluctuation heavy tails (even though a/b is decreasing) as the Gaussian component broadens (we do not detect a $a/b < 1$ out to $T = 55$ s). Thus, in an experiment, the appearance of a Gaussian C profile does not prove that the diffusion process is Fickian. One can detect non-Fickian diffusion by comparing

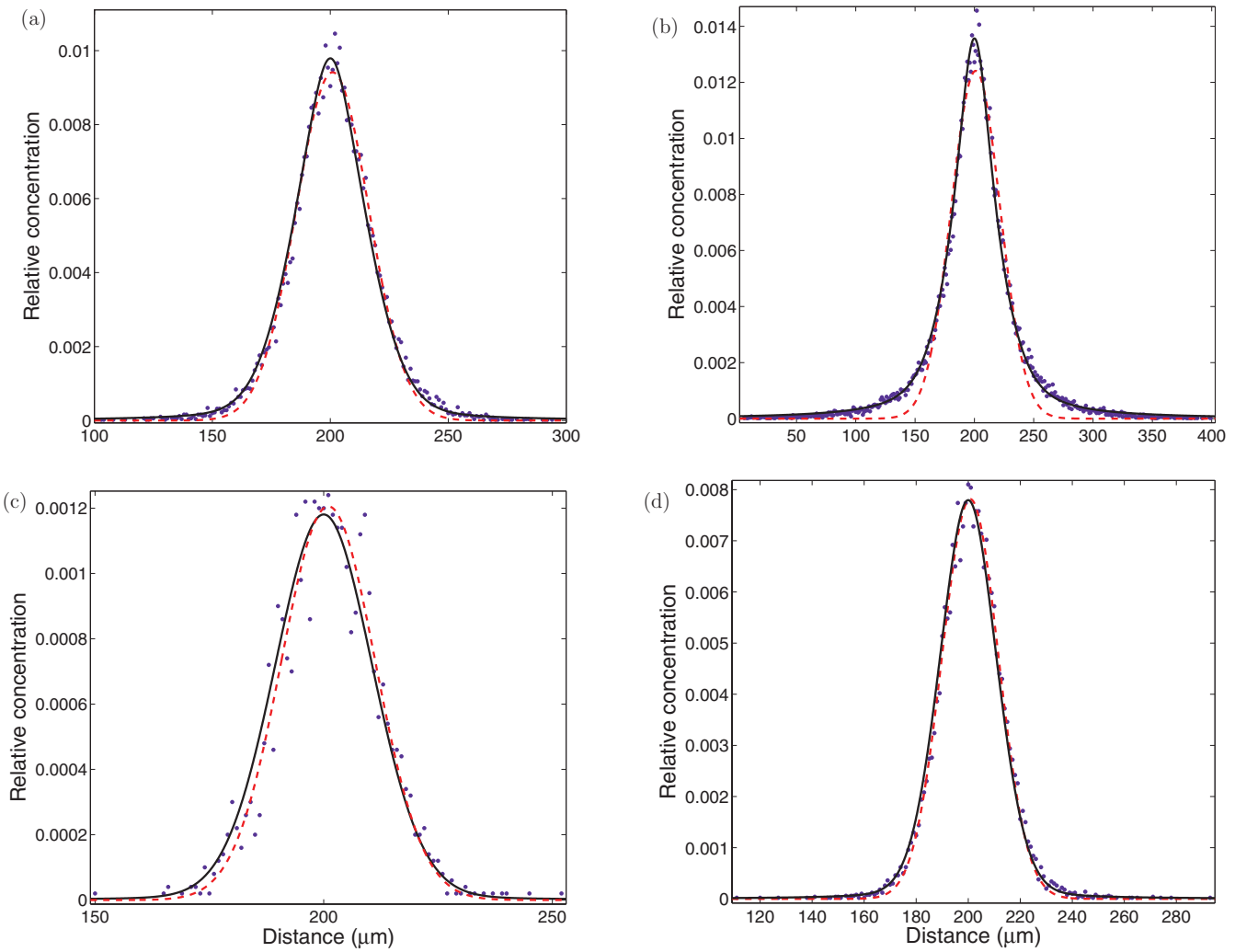

FIG. 4. (Color online) Spatially integrated (over the y axis) concentration profiles of (immobile) C particles, for Fickian diffusion at (a) $T = 2$ s and (b) $T = 15$ s and for non-Fickian diffusion with $\beta = 0.7$, $t_1 = 0.025$ s, and $t_2 = 10^4$ s at (c) $T = 2$ s and (d) $T = 15$ s. Here, the profiles are normalized by the total number of C produced at the given time. Continuous curves show best fits of the weighted sum of Gaussian (weight a) and Lorentzian (weight b) distributions. Also shown (dashed lines, in red) are pure Gaussian fits. Curves are normalized by the total number of C particles produced at the given time. Ratios of weights a/b (Gaussian/Lorentzian) are (a) 2.1, (b) 0.3, (c) 12.8, and (d) 6.0.

the C profile dynamics to calculated expectations based on normal diffusion.

Parallel analysis demonstrates that allowing the C particles to be mobile (diffusing according to the same rules as the A and B particles) for the Fickian case suppresses the fluctuations, with Gaussian behavior persisting [similar to Fig. 4(a)]. In contrast, for the non-Fickian case, the C profiles have equal weights of Gaussian and Lorentzian components.

Finally, we stress that the times and distances used in these figures offer representative behaviors; PTs determined with larger and smaller (200 and 50 μm) distances between A and B injection points yield similar behaviors to those shown here, with appropriate scaling.

Significantly, PTs with initial A and B vertical strip distribution (widths 5 μm and centers separated by 100 μm) yield the same C particle distribution behavior seen in the figures here (i.e., A and B particles bypass each other in the 2D domain); the point or strip injection is not particularly relevant. The dynamics we find are basic phenomena which account for growth of concentration fluctuations, as the species numbers decline in the reaction front.

IV. CONCLUDING REMARKS

In conclusion, we have used a particular PT method which is equivalent to solving PDEs for both Fickian and non-Fickian diffusion, depending on the choice of $\psi(t)$. The data generated by this PT are analogous to numerical solutions of these PDEs, with a suitable (but currently ill-defined) reaction term [21]. We maintain that the choice of the reaction mode in the PT is physically intuitive and avoids problematic features of volume averaging methods [21] which suppress fluctuations. In short, the PT with $\psi(t)$ and reactions is the theoretical model and the data generated are the solution. Specifically, we present a 2D study of the mixing zone dynamics of the reaction $A + B \to C$ during Fickian and non-Fickian diffusion of two species, A and B. We examine the basic pattern of the C dynamics: the temporal evolution of the spatial profile and the production of

C. The results demonstrate a similarity between the two types of diffusion, but the distinctive time scale for the non-Fickian case is very much larger even when the median transition steps are matched to the Fickian case. The spatial profile pattern is a broadening Gaussian reaction front evolving to a concentration-fluctuation dominated Lorentzian shape. The temporal production of C is fit well by a stretched exponential for both diffusion types, with the exponent for the Fickian being 2.5 times larger than for the non-Fickian. The exponents are smaller than the corresponding ones for the nonreacting case, and we assume that this reflects the attenuation of $S(t)$ due to the reactions. There are measurable quantitative differences between the two diffusion cases, which can form the basis for distinguishing between them in the analysis of experimental results.

ACKNOWLEDGMENT

This research was supported by the Israel Science Foundation (Grant No. 221/11).

[1] P. Grindrod, *Patterns and Waves: The Theory and Applications of Reaction-Diffusion Equations* (Clarendon, Gloucestershire, 1991).
[2] B. A. Grzybowski, *Chemistry in Motion: Reaction-Diffusion Systems for Micro- and Nanotechnology* (Wiley, West Sussex, 2009).
[3] L. G. Harrison, *Kinetic Theory of Living Pattern* (Cambridge University Press, Cambridge, 1993).
[4] P. J. Ortoleva, *Geochemical Self-Organization*, Oxford Monographs on Geology and Geophysics, Vol. 23 (Oxford University Press, Oxford, 1994).
[5] E. Monson and R. Kopelman, Phys. Rev. Lett. **85**, 666 (2000).
[6] A. A. Ovchinnikov and Y. B. Zeldovich, Chem. Phys. **28**, 215 (1978).
[7] M. Postma, J. Roelofs, J. Goedhart, T. W. J. Gadella, A. J. W. G. Visser, and P. J. M. Van Haastert, Mol. Biol. Cell. **14**, 5019 (2003).
[8] D. Toussaint and F. Wilczek, J. Chem. Phys. **78**, 2642 (1983).
[9] K. Kang and S. Redner, Phys. Rev. A **32**, 435 (1985).
[10] R. Dawkins and D. ben Avraham, Comput. Sci. Eng. **3**, 72 (2001).
[11] R. Erban and S. J. Chapman, Phys. Biol. **6**, 046001 (2009).
[12] B. M. Shipilevsky, Phys. Rev. E **79**, 021117 (2009).
[13] J. Palanichamy, T. Becker, M. Spiller, J. Köngeter, and S. Mohan, Comput. Visual. Sci. **12**, 51 (2009).
[14] I. Golding and E. C. Cox, Phys. Rev. Lett. **96**, 098102 (2006).
[15] Y. Sagi, M. Brook, I. Almog, and N. Davidson, Phys. Rev. Lett. **108**, 093002 (2012).
[16] S. B. Yuste, L. Acedo, and K. Lindenberg, Phys. Rev. E **69**, 036126 (2004).
[17] M. Dentz, A. Cortis, H. Scher, and B. Berkowitz, Adv. Water Resour. **27**, 155 (2004).
[18] G. Hornung, B. Berkowitz, and N. Barkai, Phys. Rev. E **72**, 041916 (2005).
[19] Y. Edery, H. Scher, and B. Berkowitz, Water Resour. Res. **46**, W07524 (2010).
[20] Y. Edery, H. Scher, and B. Berkowitz, Water Resour. Res. **47**, W08535 (2011).
[21] Y. Edery, A. Guadagnini, H. Scher, and B. Berkowitz, Adv. Water Resour. **51**, 86 (2013).
[22] M. Abramowitz and I. Stegun, *Handbook of Mathematical Functions* (Dover, New York, 1970).
[23] M. F. Shlesinger, J. Stat. Phys. **10**, 421 (1974).
[24] C. M. Gramling, C. F. Harvey, and L. C. Meigs, Environ. Sci. Technol. **36**, 2508 (2002).
[25] E. L. Cussler, *Diffusion: Mass Transfer in Fluid Systems*, 2nd ed. (Cambridge University Press, Cambridge, 1997).
[26] M. F. Shlesinger and E. W. Montroll, Proc. Natl. Acad. Sci. USA **81**, 1280 (1984).